# The Compact Integration of a Cascaded HCR Circuit for Highly Reliable Cancer Cells Discrimination

*Pei Dong†,[a] Ruomeng Li†,[a] Shizhen He†,[a] Qingqing Zhang,[a] Jinhua Shang,[a] Yuqian Jiang,[a] Xiaoqing Liu,[a,b] Fuan Wang*[a,b]*

a College of Chemistry and Molecular Sciences, Wuhan University, 430072 Wuhan, P. R. China.

b Research Institute of Shenzhen, Wuhan University, Shenzhen, 518057, P. R. China Email: fuanwang@whu.edu.cn

* To whom correspondence should be addressed. E-mail: fuanwang@whu.edu.cn

† P. Dong, R. Li and S. He contributed equally.

# Table of Contents

## EXPERIMENTAL SECTION

### Materials.

Sodium chloride, magnesium chloride, and 4-(2-Hydroxyethyl)piperazine-1-ethanesulfonic acid sodium salt (HEPES) were purchased from Sigma-Aldrich (MO, USA). All oligonucleotides were synthesized and HPLC-purified by Sangon Biotech. Co., Ltd. (Shanghai, China). The sequences of these oligonucleotides are listed in **Table S1**, **Table S2,** and **Table S3**. Ultrapure water was obtained from a Millipore Milli-Q water purification system and then used throughout the experiments. Lipofectamine 3000 transfection reagent (lipo-3000) was obtained from Invitrogen (Carlsbad, CA).

### Fluorescence assay.

Each DNA hairpin (4 μM) was annealed in reaction buffer (10 mM HEPES, 1 M NaCl, and 50 mM $MgCl_2$, pH 7.2) at 95 ℃ for 5 min, and then rapidly cooled down to room temperature (25 ℃) for 2 hours before use.

To detect the DNA targets using the CCH circuit, DNA hairpin mixtures (100 nM $\mathbf{H_1}$, 200 nM $\mathbf{H_2}$) were incubated with two DNA targets (**I** and **T**, 50 nM each) at 25 ℃ for 2.5 h. Afterwards, the fluorescence spectra of TAMRA (for tracing upstream CHA circuit) were collected from 570 to 650 nm at a fixed excitation of 557 nm, and the fluorescence spectra of ROX (for tracing the CCH circuit) were collected from 600 to 700 nm upon a fixed excitation of 586 nm. The different **I** concentration-dependent fluorescence changes of the CCH circuit were obtained by incubating the two hairpins (100 nM $\mathbf{H_1}$, 200 nM $\mathbf{H_2}$) and fixed concentration of **T** (100 nM) with different concentrations of **I** at 25 ℃ for 2.5 h. The different **T** concentration-dependent fluorescence changes were acquired by incubating 100 nM $\mathbf{H_1}$, 200 nM $\mathbf{H_2}$, and 50 nM **I** with different concentrations of **T** at 25 ℃ for 2.5 h. All concentration-dependent fluorescence spectra were collected from the fluorescence spectra of ROX. To verify the performance of three-hairpin CHA-HCR system for DNA targets detection, the DNA hairpins solution containing 100 nM $\mathbf{H_1'}$, 200 nM $\mathbf{H_2'}$, and 100 nM $\mathbf{H_3'}$ was incubated with two DNA targets (50 nM **I** and 50 nM **T**) at 25 ℃ for 200 min.

To detect the microRNA (miRNA) targets using the CCH circuit, the prepared hairpins solution ($\mathbf{mH_1}$, $\mathbf{mH_2}$, 100 nM each) was incubated with two miRNA targets (miR-155 and miR-21, 50 nM each) at 25 ℃ for 1 h. The corresponding fluorescence spectra of TAMRA and ROX were collected. The different miR-155 and/or miR-21 concentration-dependent fluorescence changes of the miRNA-targeted CCH circuit were obtained by incubating the two hairpins ($\mathbf{mH_1}$, $\mathbf{mH_2}$, 100 nM each) and fixed concentration of miR-21 and/or miR-155 (50 nM) with different concentrations of miR-155 and/or miR-21 at 25 ℃ for 1 h. To verify the performance of three-hairpin CHA-HCR system for miRNAs detection, the hairpins solution containing (200 nM $\mathbf{mH_1'}$, 200 nM $\mathbf{mH_2'}$, 200 nM $\mathbf{mH_3'}$) was incubated with two miRNA targets (miR-155 and miR-21, 50 nM each) at 25 ℃ for 200 min.

**Electrophoresis assay.**

Hairpin mixtures (**$H_1$** and **$H_2$**, 400 nM each) were incubated with or without DNA targets (**I** and **T**, 50 nM each) at 25 ℃ for 2.5 h. Afterwards, each sample was added with 2 μL of 6×loading buffer and gently loaded into the 9% native polyacrylamide gel. Then the electrophoresis was performed in 1×TBE buffer at 150 V for 3 h. The gel was stained with diluted GelRed$^{TM}$ solution for 10 min and imaged by a FluorChem FC3 (Protein-Simple, USA) under UV irradiation (365 nm).

**Atomic force microscopy imaging.**

A prepared mica was dropped with 5 mM $MgCl_2$ for 5 min to obtain positive charges and gently soaked in distilled water. After drying in air, the CCH products were diluted with 20 mM HEPES buffer (pH 7.2), followed by depositing onto the modified mica surface for 15 min. The sample was dried under a stream of nitrogen, and then was scanned in tapping mode by Multimode-8 Atomic Force Microscopy (AFM) with a NanoScope V controller (Bruker).

**Cytotoxicity assay.**

MCF-10A cells ($10^4$ cells) were incubated in a 96-well plate with an MCF-10A cell-specific culture medium (DMEM/F12, NEAA, insulin, hydrocortisone, 5% HS, 1% P/S solution, and 20 ng/mL EGF) and cultured at 37 ℃ for 36 h. Then the cells were incubated with different concentrations (0, 25, 50, 100, 200, and 400 nM) of CCH probes (1 μL of **$mH_1$** and **$mH_2$**, 100 μM each) for 24 h. Afterwards, the cells were washed with PBS three times to remove the redundant DNA probes, and incubated with 150 μL of 3-(4,5-dimethylthialzol-2-yl)-2,5-diphenyltetrazolium bromide (MTT) solution (0.5 mg/mL) for 4 h in the dark at 37 ℃. After removing the MTT solution gently, 150 μL of DMSO solution was added to each well to dissolve the formed formazan crystals. The absorbance at the wavelength of 570 nm was measured by a microplate reader.

**Cell culture and transfection for confocal microscopy imaging.**

MDA-MB-231 cells, MCF-7 cells, and A549 cells were cultured in Dulbecco's Modified Eagle Medium (DMEM) supplemented with 10% fetal bovine serum (FBS) and 1% penicillin/streptomycin. MCF-10A cells were grown in an MCF-10A cell-specific culture medium. All cells were plated in 20 mm cell culture dishes and grown overnight at 37 ℃ in a 5% $CO_2$ atmosphere.

Transfection experiment of the CCH circuit was performed according to the subsequent manufacturer's protocol. Phosphorothioate-modified reactants of the CCH circuit were used to improve stability in living cells. Firstly, the CCH reactants (1 μL of **$mH_1$** and **$mH_2$**, 100 μM each) in 200 μL of Opti-MEM were gently mixed with lipo-3000 (3 μL) in 200 μL of Opti-MEM for 10 min. Then the cultured cells were transfected with the 400 μL of above mentioned Opti-MEM mixture supplied with 80 μL FBS at 37 ℃ for 4 h. Subsequently, the cells were washed three times with cold phosphate buffered saline (PBS buffer) and incubated in 1 mL of DMEM for imaging after incubating with Hoechst 33342 for 8 min. For the downregulation of miRNAs assays, MDA-MB-231 cells were pre-transfected with the 100 nM anti-miRNA sequences (anti-miR-155 and/or anti-miR-21, 1 μL each) for 1 h, and then further transfected with the CCH

reactants (1 μL of **mH$_1$** and **mH$_2$**, 100 μM each). The transfection procedure of three-hairpin CHA-HCR system was similar to that of CCH circuit, but the reactants of three-hairpin CHA-HCR system were 1 μL of **mH$_1$'**, **mH$_2$'**, and **mH$_3$'** (100 μM each). The transfection procedure of HCR system was similar to that of CCH circuit, but the reactants of HCR system were 1 μL of **mH$_1$''** and **mH$_2$''** (100 μM each).

All fluorescence imaging assays were performed by a Leica TCS SP8 confocal laser scanning microscope (CLSM). The red channel of TAMRA was obtained using an external 561 nm excitation. The green channel of ROX was obtained using an external 586 nm excitation. All of the cell fluorescence images were analyzed by using ImageJ software.

**Flow cytometric analysis.**

MDA-MB-231 cells ($10^5$ cells) were cultured in 12-well microplates with 1 mL DMEM medium for 24 h. Then the cells were transfected with the CCH system (1 μL of **mH$_1$** and **mH$_2$**, 100 μM each) at different time points (0, 0.5, 1, 2, 3, 4, and 5 h). Afterwards, cells were washed with cold PBS buffer three times and incubated with 300 μL of trypsin for 3 min. Then the cells were washed with cold PBS buffer three times and centrifuged at 1500 rpm for 3 min, followed by resuspending in PBS buffer for flow cytometry analysis.

MDA-MB-231 cells, MCF-7 cells, and A549 cells ($10^5$ cells) were cultured in 12-well microplates with 1 mL DMEM medium for 24 h. MCF-10A cells ($10^5$ cells) were cultured in 12-well microplates with 1 mL MCF-10A cell-specific culture medium for 24 h. Then the cells were transfected with the CCH system (1 μL of **mH$_1$** and **mH$_2$**, 100 μM each) for 4 h. Afterwards, cells were washed with cold PBS buffer three times and incubated with 300 μL of trypsin for 3 min. Then the cells were washed with cold PBS buffer three times and centrifuged at 1500 rpm for 3 min, followed by resuspending in PBS buffer for flow cytometry analysis. The fluorescence intensities of cells were tested, and the data were analyzed by FlowJo software.

**Table S1. The DNA sequences of CHA-control-HCR (CCH) system.**

| Name | Sequence (5'→3') |
|---|---|
| **$H_1$** | 5'-BHQ2-GCT TCA TCT TCA TCT CCG ACA CTC CGG AGA TGA AGA T(ROX) GA AGC ACG AAG TCT TAG TGG AAT TAT GTC GGT AGG TAG GTA GAA CAT AAT TCC ACT AAG AAC AGG G-TAMRA-3' |
| **$H_2$** | 5'-CGG TAG GTA GGT AGA GAG TGT CGG AGA TGA AGA TGA AGC CTT CGT GCT TCA TCT TCA TCT CCG TTT TAT CTT AGT GGA ATT ATG TTC TAC CTA CCT ACC GAC ATA AT-3' |
| **I** | 5'-CCC TGT TCT TAG TGG AAT TAT GT-3' |
| **$I_a$** | 5'-CC**A** TGT TCT TAG TGG AAT TAT GT-3' |
| **$I_b$** | 5'-CC**A** TGT TCT **A**AG TGG AAT TAT GT-3' |
| **$I_c$** | 5'-CC**A** TGT TCT **A**AG TGG AA**A** TAT GT-3' |
| **T** | 5'-GCT TCA TCT TCA TCT CCG ACA CTC-3' |
| **$T_a$** | 5'-GCT TCA TCT TCA TCT CCG AC**G** CTC-3' |
| **$T_b$** | 5'-GCT TCA TCT TCA TC**G** CCG AC**G** CTC-3' |
| **$T_c$** | 5'-GCT TCA **G**CT TCA TC**G** CCG AC**G** CTC-3' |
| **$mH_1$** | 5'-BHQ2-TAG CTT ATC AGA CTG AGT GTT GAT CAG TCT GA T(ROX) AAG CTA ACC CTC CTA ATC GTG ATA GGG GTC GGT AGG TAG GTA GAA CCC CTA TCA CGA TTA GCA TTA A-TAMRA-3' |
| **$mH_2$** | 5'-CGG TAG GTA GGT AGA GGT CAA CAT CAG TCT GAT AAG CTA GAG GGT TAG CTT ATC AGA CTG AAA AAA CTA ATC GTG ATA GGG GTT CTA CCT ACC TAC CGA CCC CTA-3' |
| **miR-21** | 5'-UAG CUU AUC AGA CUG AUG UUG A-3' |
| **miR-155** | 5'-UUA AUG CUA AUC GUG AUA GGG GU-3' |
| **let-7a** | 5'-UGA GGU AGU AGG UUG UAU AGU U-3' |
| **miR-199a** | 5'-ACA GUA GUC UGC ACA UUG GUU A-3' |
| **miR-429** | 5'-UAA UAC UGU CUG GUA AAA CCG U-3' |
| **miR-155 inhibitor** | 5'-mA* mC* mC* mC mC mU mA mU mC mA mC mG mA mU mU mA mG mC mA mU mU* mA* mA*-3' |
| **miR-21 inhibitor** | 5'-mU* mC* mA* mA mC mA mU mC mA mG mU mC mU mG mA mU mA mA mG* mC* mU * mA-3' |

* indicates phosphorothioate bond.

**Table S2. The DNA sequences of three-hairpin CHA-HCR system.**

| Name | Sequence (5'→3') |
|---|---|
| **$H_1$'** | 5'-TCT TAG TGG AAT TAT GTC GGT AGG TAG GTA GAA CAT AAT TCC ACT AAG AAC AGG G-3' |
| **$H_2$'** | 5'-CGG TAG GTA GGT AGA GAG TGT CGG AGA TGA AGA TGA AGC CTT CGT GCT TCA TCT TCA TCT CCG TTT TAT CTT AGT GGA ATT ATG TTC TAC CTA CCT ACC GAC ATA AT-3' |
| **$H_3$'** | 5'-BHQ2-GCT TCA TCT TCA TCT CCG ACA CTC CGG AGA TGA AGA T(ROX) GAA GCA CGA AG-3' |
| **I** | 5'-CCC TGT TCT TAG TGG AAT TAT GT-3' |
| **T** | 5'-GCT TCA TCT TCA TCT CCG ACA CTC-3' |
| **m$H_1$'** | 5'-CTA ATC GTG ATA GGG GTC GGT AGG TAG GTA GAA CCC CTA TCA CGA TTA GCA TTA A-3' |
| **m$H_2$'** | 5'-CGG TAG GTA GGT AGA GGT CAA CAT CAG TCT GAT AAG CTA GAG GGT TAG CTT ATC AGA CTG AAA AAA CTA ATC GTG ATA GGG GTT CTA CCT ACC TAC CGA CCC CTA-3' |
| **m$H_3$'** | 5'-BHQ2-TAG CTT ATC AGA CTG AGT GTT GAT CAG TCT GA T(ROX) AAG CTA ACC CTC-3' |
| **miR-21** | 5'-UAG CUU AUC AGA CUG AUG UUG A-3' |
| **miR-155** | 5'-UUA AUG CUA AUC GUG AUA GGG GU-3' |

**Table S3. The DNA sequences of HCR system.**

| Name | Sequence (5'→3') |
|---|---|
| **m$H_1$''** | 5'-GGT CAA CAT CAG TCT GAT AAG CTA GAG GGT TAG CTT ATC AGA CTG A-3' |
| **m$H_2$''** | 5'- BHQ2-TAG CTT ATC AGA CTG AGT GTT GAT CAG TCT GAT(ROX) AAG CTA ACC CTC -3' |
| **miR-21** | 5'-UAG CUU AUC AGA CUG AUG UUG A-3' |

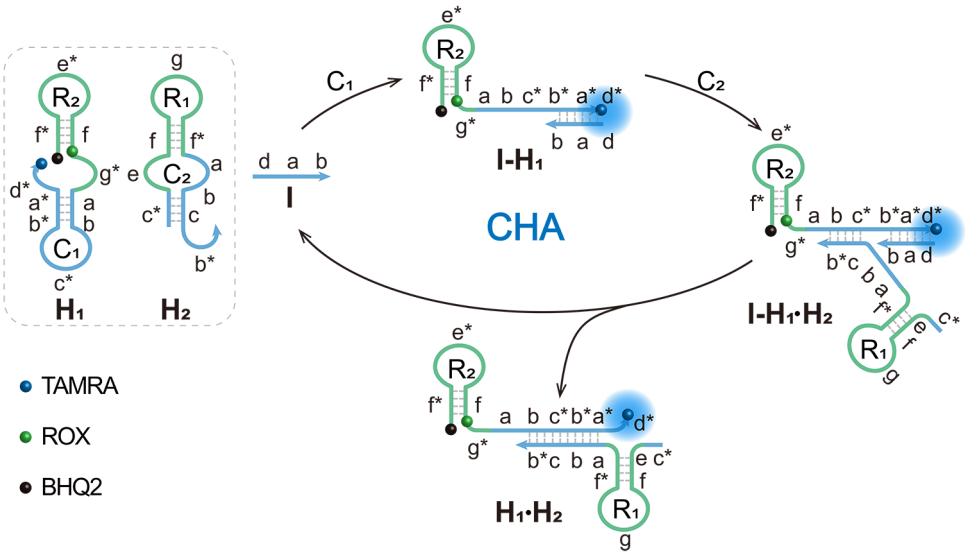


**Figure S1.** Principle of upstream CHA circuit.

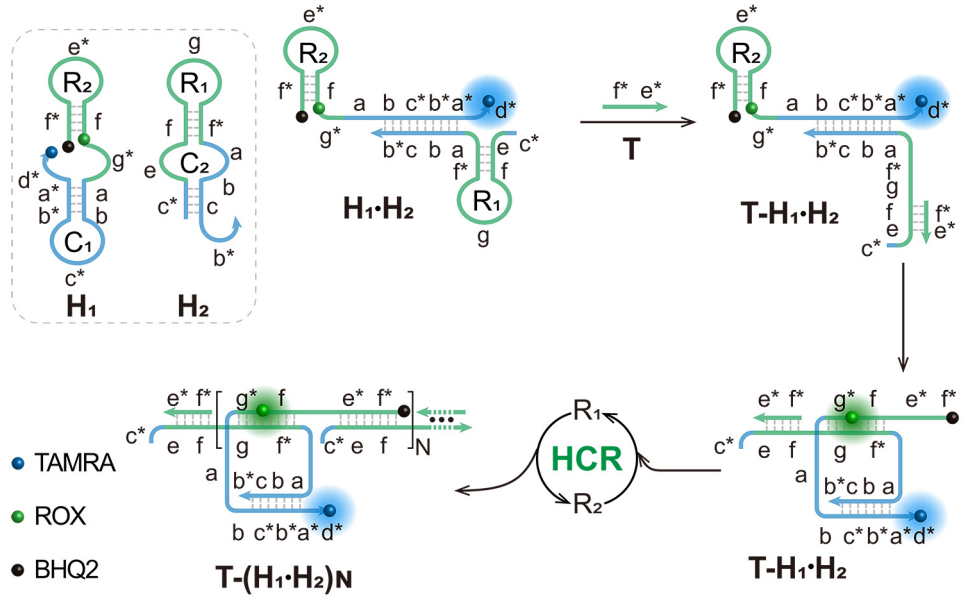


**Figure S2.** Principle of downstream HCR circuit.

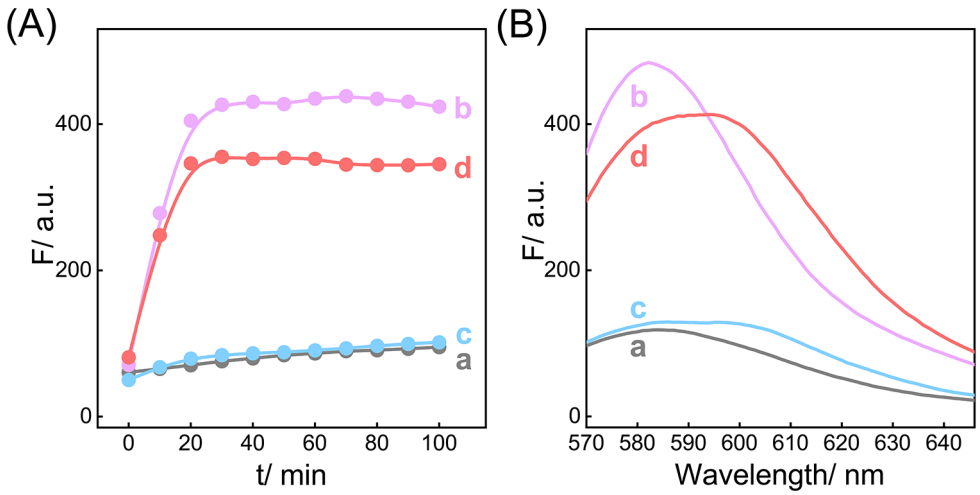


**Figure S3.** Feasibility verification of the CCH circuit for DNA targets detection. (A) Fluorescence kinetic characterization (TAMRA) of the CCH circuit under different conditions with 100 nM $\mathbf{H_1}$ and 200 nM $\mathbf{H_2}$: (a) no **I** and **T**, (b) 50 nM **I**, (c) 50 nM **T**, (d) 50 nM **I** and **T**. (B) The corresponding fluorescence spectra from **Figure S3A**.

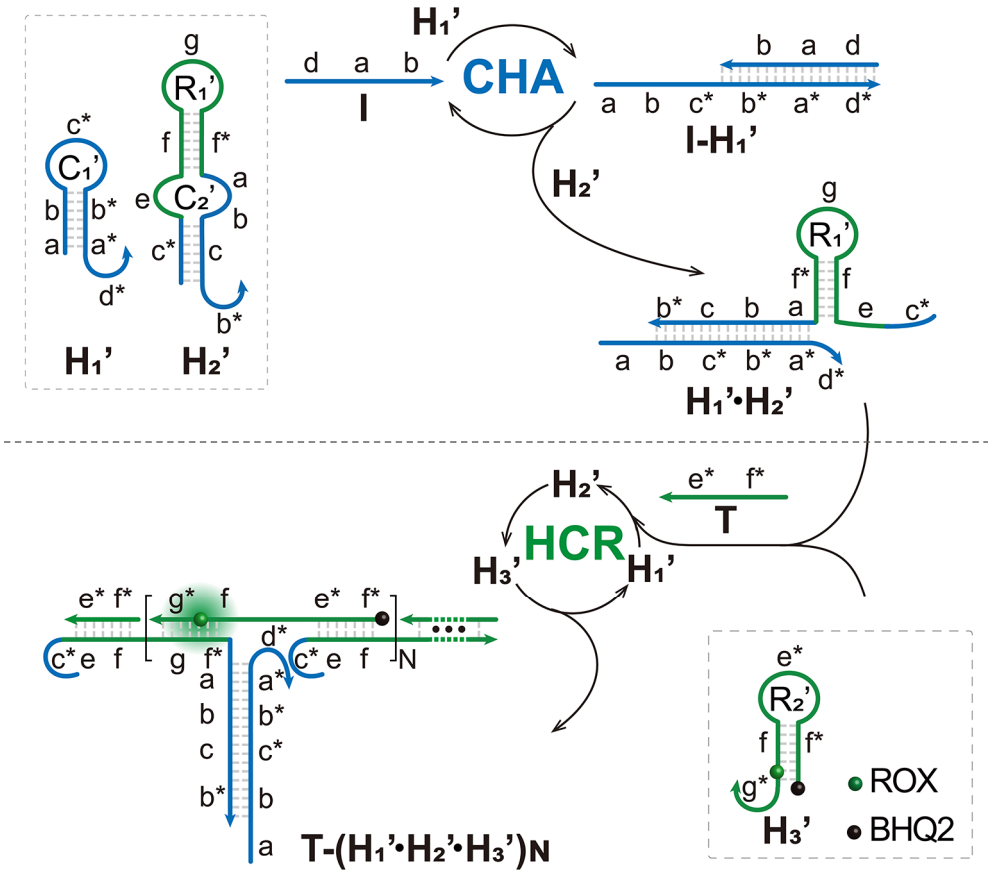


**Figure S4.** Principle of three-hairpin CHA-HCR system for detecting DNA targets.

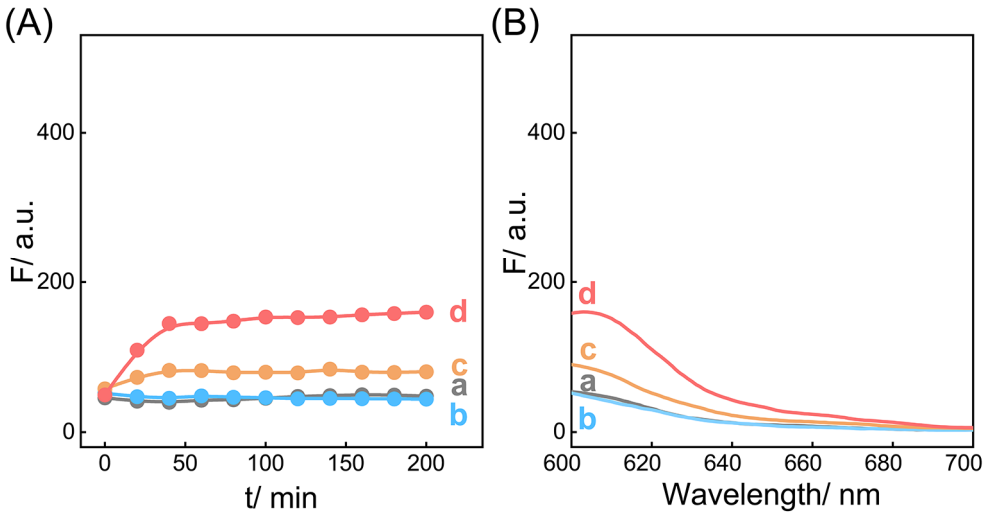


**Figure S5.** Feasibility verification of the traditional three-hairpin CHA-HCR system. (A) Fluorescence kinetic characterization (ROX) of the three-hairpin CHA-HCR system under different groups with 100 nM **H₁'**, 100 nM **H₂'**, and 200 nM **H₃'**: (a) no **I** and **T**, (b) 50 nM **I**, (c) 50 nM **T**, (d) 50 nM **I** and **T**. (B) The corresponding fluorescence spectra from **Figure S5A**.

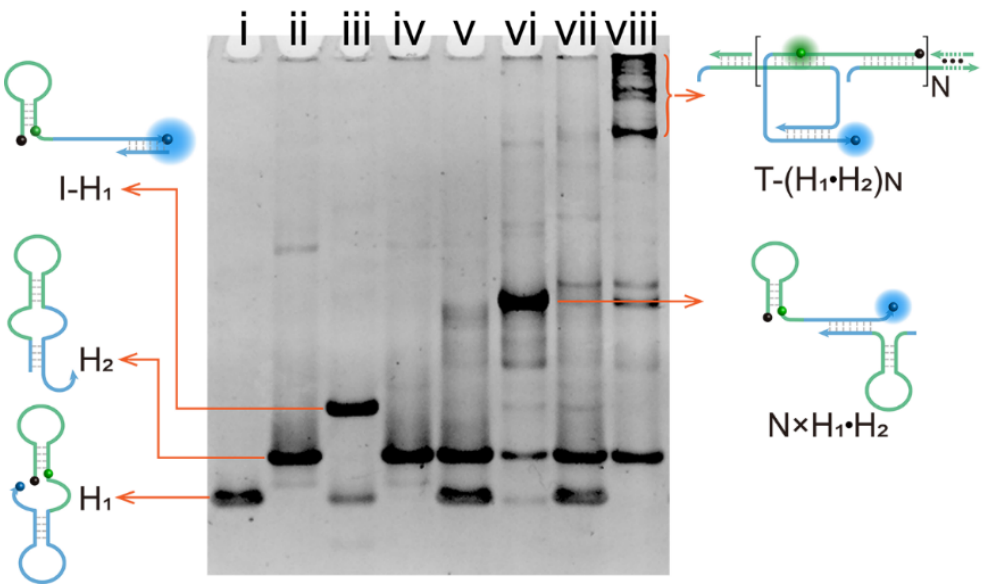


**Figure S6.** Native PAGE image labeled with the DNA structure of the CCH circuit: (i) $\mathbf{H_1}$, (ii) $\mathbf{H_2}$, (iii) $\mathbf{H_1}$ + **I**, (iv) $\mathbf{H_2}$ + **T**, (v) $\mathbf{H_1}$ + $\mathbf{H_2}$, (vi) $\mathbf{H_1}$ + $\mathbf{H_2}$ + **I**, (vii) $\mathbf{H_1}$ + $\mathbf{H_2}$ + **T**, and (viii) $\mathbf{H_1}$ + $\mathbf{H_2}$ + **I** + **T**.

As shown in **Figure S7**, with the addition of **T** (lane **iii**), $\mathbf{H_1}$ remained unchanged as individual $\mathbf{H_1}$ (lane **i**), indicating that only $\mathbf{H_1}$ could not be opened by **T** to produce redundant hybridization. Similarly, with the introduction of **I** (lane **iv**), $\mathbf{H_2}$ remained unchanged as individual $\mathbf{H_2}$ (lane **ii**), indicating that mere $\mathbf{H_2}$ will not be opened by **I** to produce redundant hybridization. Thus, these results indicated that $\mathbf{H_1}$, **T** and $\mathbf{H_2}$, **I** will not produce redundant hybridization.

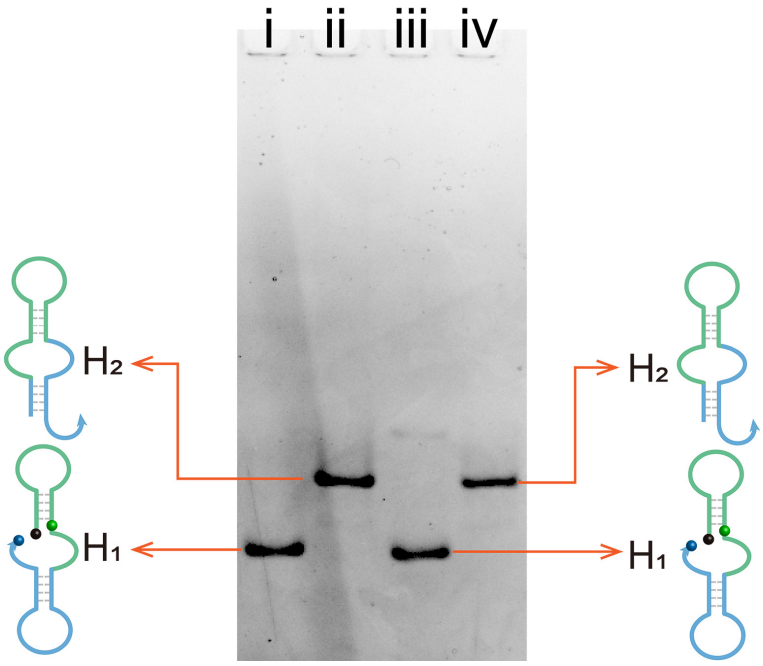


**Figure S7.** Native PAGE image of the CCH circuit: (i) $\mathbf{H_1}$, (ii) $\mathbf{H_2}$, (iii) $\mathbf{H_1}$ + **T**, and (iv) $\mathbf{H_2}$ + **I**.

In the CCH circuit, the different concentration ratios of two hairpins impact the amplification efficiency of CCH circuit. Thus, we optimized the concentration ratio of $\mathbf{H_1}$ and $\mathbf{H_2}$ (1:1, 1:2, 1:3, and 2:1). As shown in **Figure S8A**, a higher signal-to-background (S/B) ratio of $\mathbf{H_1}$ to $\mathbf{H_2}$ in the CCH circuit was acquired from the concentration ratio of $\mathbf{H_1}$ and $\mathbf{H_2}$ fixed as 1:2.

The reaction temperature is vital to the stability of the DNA hybridization, thus determining the performance of the CCH circuit to some extent. As a result, we carried out the CCH circuit at different temperatures (25 ℃ and 37 ℃) to investigate the relation between the temperature and the S/B ratio of the CCH circuit. As shown in **Figure S8B**, a higher S/B ratio was performed at 25 ℃, thus we chose 25 ℃ for the subsequent experiments.

The salt concentrations of reaction buffer are also key to the stability of DNA hairpins and dsDNA structures. Therefore, we studied the relation between salt concentrations of reaction buffer and the S/B ratio using different NaCl concentrations (100 mM and 1 M) in 10 mM HEPES buffer. As shown in **Figure S8C**, the HEPES buffer containing 1 M NaCl generated a higher S/B ratio. Thus, the 1 M NaCl-contained HEPES buffer was selected as the optimized reaction buffer for the following experiments.

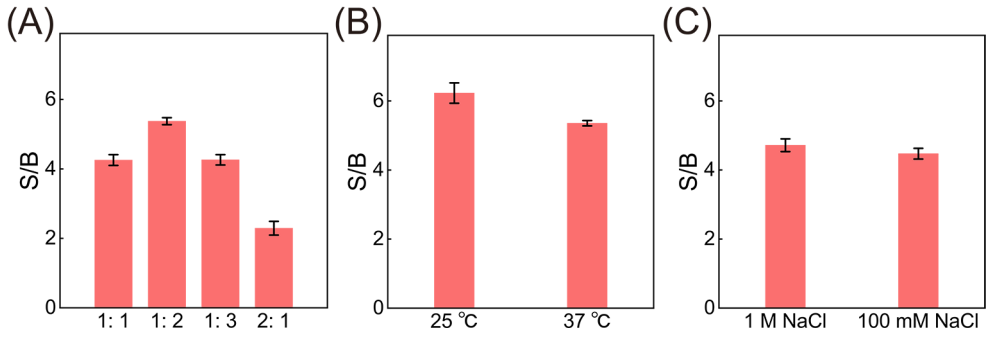


**Figure S8.** Optimization of reaction conditions for DNA detection using CCH circuit. (A) The signal-to-background (S/B) ratio of the CCH circuit with different ratios of $\mathbf{H_1}$ to $\mathbf{H_2}$ (1:1, 1:2, 1:3, and 2:1). (B) The S/B ratio of the CCH circuit implemented in different temperatures (25 ℃ and 37 ℃). (C) The S/B ratio of the CCH circuit in reaction buffer (10 mM HEPES, 50 mM $MgCl_2$, pH 7.2) containing different NaCl concentrations (1 M and 100 mM). Error bars represent one standard deviation for three independent experiments.

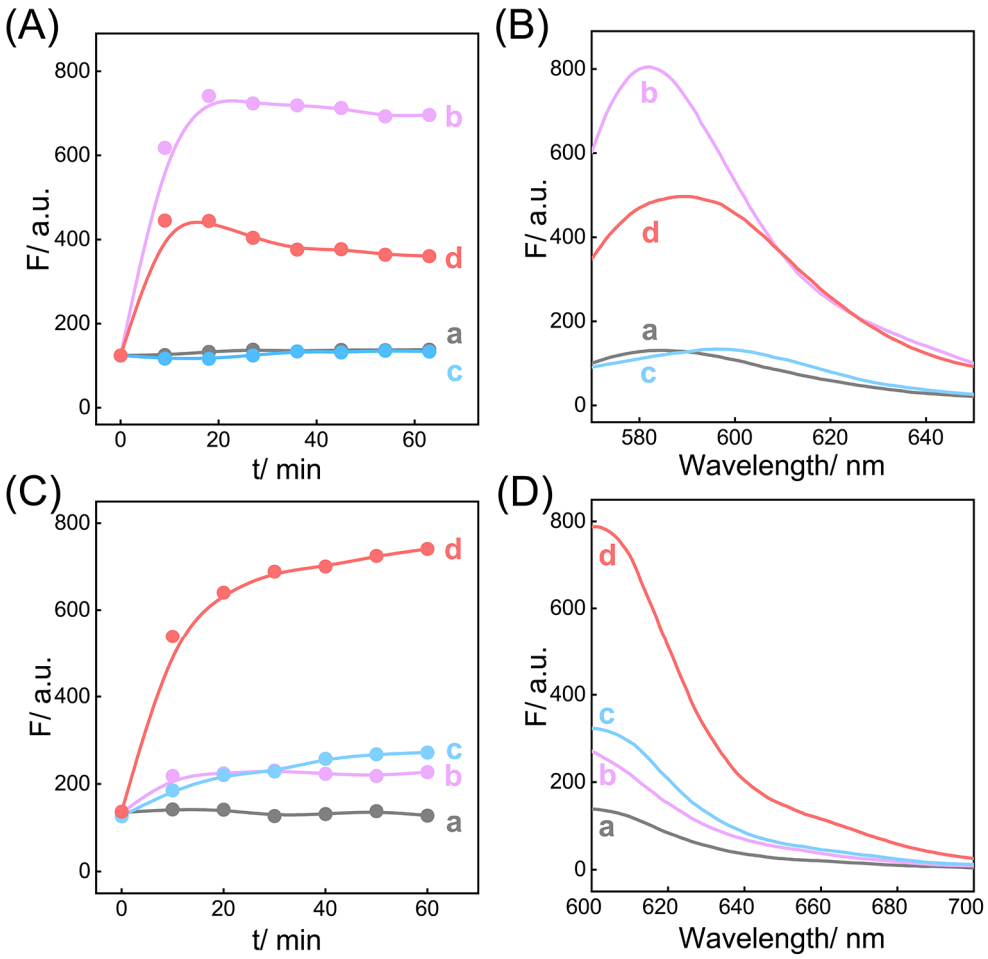


**Figure S9.** Feasibility verification of the CCH circuit for miRNAs detection. (A) Time-dependent fluorescence (TAMRA) of the CCH circuit consists of different groups with 100 nM **mH$_1$** and 100 nM **mH$_2$**: (a) no miR-155 and miR-21, (b) 50 nM miR-155, (c) 50 nM miR-21, (d) 50 nM miR-155 and miR-21. (B) The corresponding fluorescence spectra from **Figure S9A**. (C) Time-dependent fluorescence (ROX) of the CCH circuit consists of different groups with 100 nM **mH$_1$** and 100 nM **mH$_2$**: (a) no miR-155 and miR-21, (b) 50 nM miR-155, (c) 50 nM miR-21, (d) 50 nM miR-155 and miR-21. (D) The corresponding fluorescence spectra from **Figure S9C**.

The corresponding control group, three-hairpin CHA-HCR circuit, is also designed for detecting miRNAs. MiR-155 and miR-21 could trigger upstream CHA and downstream HCR, respectively. Meanwhile, the sequences of **$H_1$**, **$H_2$**, and **$H_3$** replaced for miRNA sequences, named **$mH_1$'**, **$mH_2$'** (**$mC_2$'-$mR_1$'**), and **$mH_3$'**. As shown in **Figure S10A**, miR-155 opens **$mH_1$'** to trigger CHA circuit, then miR-21 opens **$mR_1$'** and executes HCR circuit with enhanced fluorescence of ROX. As shown in **Figure S10B**, a weak fluorescence response was observed and a long time was consumed (200 min) for the complete reaction compared to the CCH circuit (**Figure S9**). The corresponding fluorescence spectra of ROX (**Figure S10C**) were consistent with fluorescence kinetic curves. These results further indicated that the satisfactory sensing performance of our compact CCH circuit.

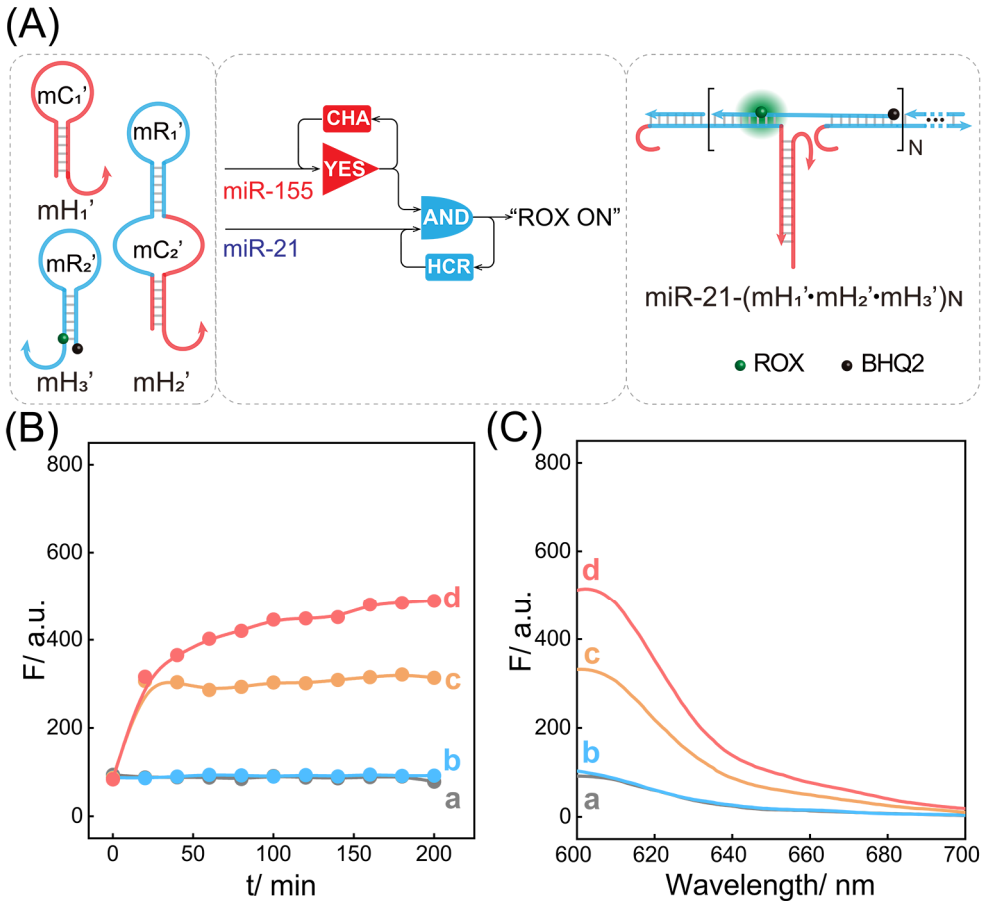


**Figure S10.** Feasibility verification of the three-hairpin CHA-HCR system. (A) Brief principle of the three-hairpin CHA-HCR system for amplified miR-155 and miR-21 detection. (B) Time-dependent fluorescence (ROX) of the three-hairpin CHA-HCR system consists of different groups with 200 nM **$mH_1$**, 200 nM **$mH_2$'**, and 200 nM **$mH_3$'**: (a) no miR-155 and miR-21, (b) 50 nM miR-155, (c) 50 nM miR-21, (d) 50 nM miR-155 and miR-21. (C) The corresponding fluorescence spectra from **Figure S10B**.

In the miRNA-targeted CCH circuit, we investigated the effect of the concentration ratios of **mH$_1$** and **mH$_2$** (1:1, 1:2, 1:3, and 2:1) on the S/B ratio of the miRNA-targeted CCH circuit. As shown in **Figure S11A**, a higher S/B ratio of **mH$_1$** to **mH$_2$** in the miRNA-targeted CCH circuit was obtained from 1:1-fixed concentration ratio of **mH$_1$** and **mH$_2$**. Then we carried out the CCH circuit at different temperatures (25 ℃ and 37 ℃) to study the influence of the temperatures on the S/B ratio of the miRNA-targeted CCH circuit. As shown in **Figure S11B**, a higher S/B ratio was performed at 25 ℃, thus we chose 25 ℃ for the subsequent experiments. Lastly, we investigated the effect of salt concentrations of reaction buffer on the S/B ratio using different NaCl concentrations (100 mM and 1 M) in 10 mM HEPES buffer. As shown in **Figure S11C**, the 100 mM NaCl-contained HEPES buffer generated a higher S/B ratio. Thus, 100 mM NaCl-contained HEPES buffer was selected as the optimized reaction buffer for the following experiments.

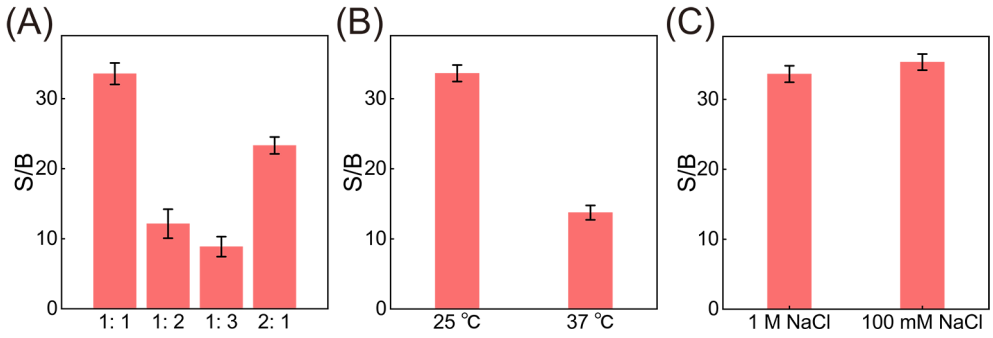


**Figure S11.** The optimization of reaction conditions for miRNAs detection using miRNA-targeted CCH circuit. (A) The S/B ratio of the miRNA-targeted CCH circuit with different ratios of **mH$_1$** to **mH$_2$** (1:1, 1:2, 1:3, and 2:1). (B) The S/B ratio of the miRNA-targeted CCH circuit implemented in different temperatures (25 ℃ and 37 ℃). (C) The S/B ratio of the miRNA-targeted CCH circuit in reaction buffer (10 mM HEPES, 50 mM $MgCl_2$, pH 7.2) containing different NaCl concentrations (1 M and 100 mM). Error bars represent one standard deviation for three independent experiments.

The stability of the miRNA-targeted CCH circuit is pivotal to detect miRNAs in complex biological environment. Therefore, some diluted serums were used as reaction buffers to investigate the stability of the current circuit. The circuit was carried out in the reaction buffer containing varied serums (0%, 5%, and 10% serum buffers). As shown in **Figure S12**, the performances of the CCH circuit in different diluted serums were almost same with that in buffer, indicating that the circuit can keep stable in biological environment.

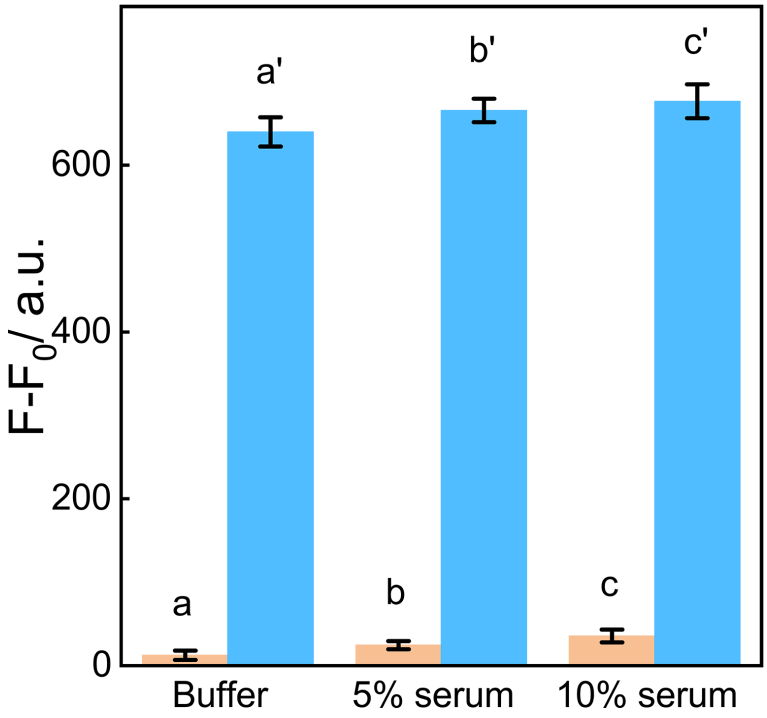


**Figure S12.** Stability of the CCH circuit in serum samples. Fluorescence changes generated by the circuit in the absence (a, b, c) and in the presence (a', b', c') of miR-155 and miR-21 under the reaction buffer containing varied serums (0%, 5%, and 10% serum buffers). Error bars represent one standard deviation for three independent experiments.

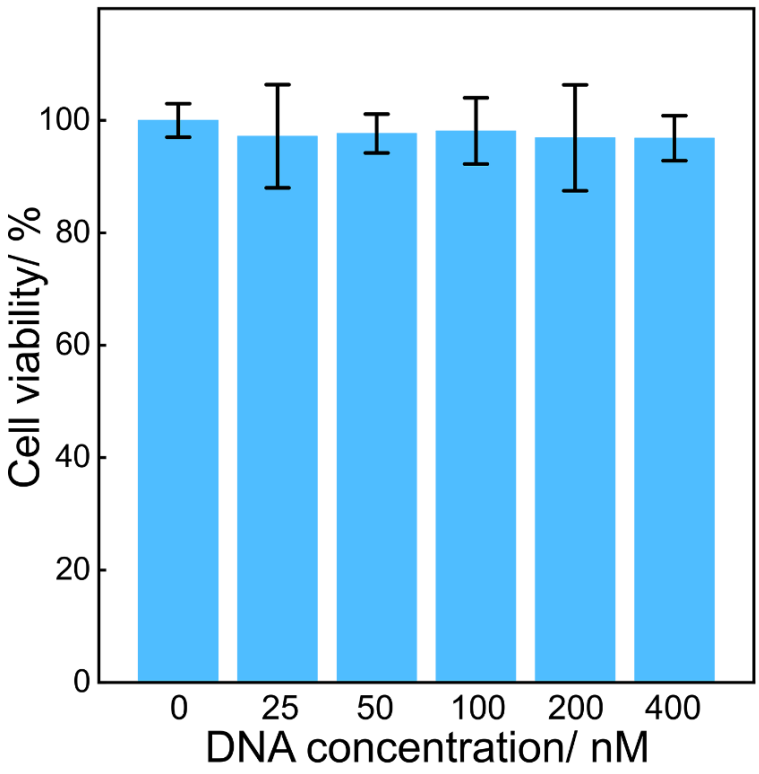


**Figure S13.** Cytotoxicity study of the CCH circuit by cell proliferation assay. The cell viability values (%) are determined by incubating MCF-10A cells with CCH probes of varied concentrations (0-400 nM) for 24 h. Error bars represent one standard deviation for three independent experiments.

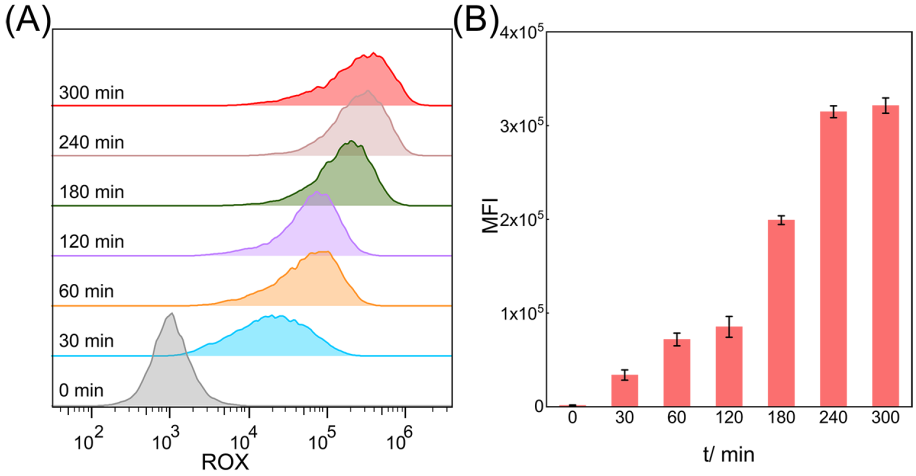


**Figure S14.** Optimization of incubation time for living cells imaging. (A) Flow cytometry analysis of the CCH-treated MDA-MB-231 cells at different incubation times. (B) The corresponding Mean Fluorescence Intensity (MFI) histogram of the flow cytometry results from **Figure S14A**. Error bars represent one standard deviation for three independent experiments.

The single-staged HCR circuit is limited with intrinsic low amplification ability, which might induce undesirable imaging performance of low abundant biomarkers. Compared with the single-staged HCR system, our cascaded CCH system is constructed with two circuit constitutes (CHA circuit and HCR circuit), which could increase the overall amplification capacity with an improved signal transduction, and thus achieve an improved imaging performance (**Figure S15A**). A faint fluorescence was obtained in HCR-treated MDA-MB-231 cells (**Figures S15B** and **S15C**), yet an obvious fluorescence was acquired in CCH-treated MDA-MB-231 cells (**Figures S15D** and **S15E**), demonstrating that the cascaded CCH system can achieve more sensitive and accurate intracellular imaging in living cells than the single-staged HCR system.

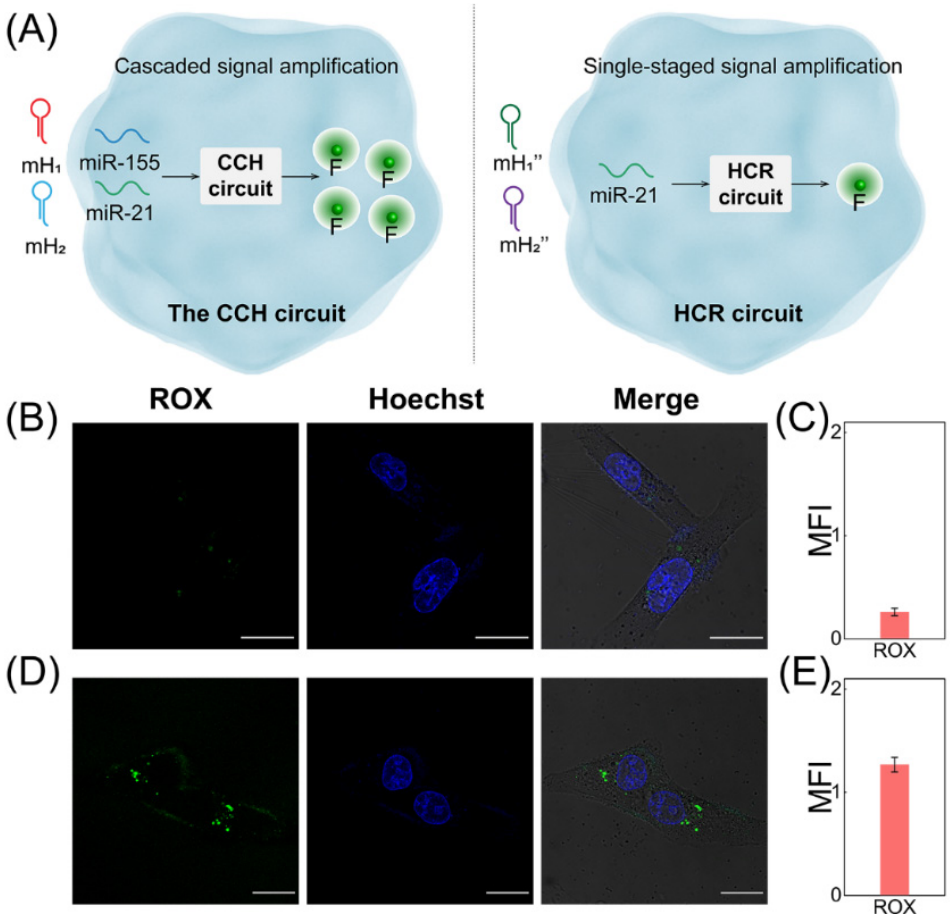


**Figure S15.** Imaging of the CCH system and HCR system. (A) The schematic illustration of probes delivery for the CCH system and HCR system. (B) CLSM images of MDA-MB-231 cells treated with the HCR system. (C) The corresponding statistical histogram of MFI from **Figure S15B**. (D) CLSM images of MDA-MB-231 cells treated with the CCH system. (E) The corresponding statistical histogram of MFI from **Figure S15D**. Scale bar: 20 μm. Error bars represent one standard deviation for three independent experiments.

The cascaded three-hairpin CHA-HCR circuit could achieve an improved sensing performance in contrast to the single-staged HCR circuit, yet introduced new problems including the poor cell-delivering uniformity and possible undesired crosstalk between these multiple components. Our homogeneous CCH system could improve the delivery efficiency of the DNA probes by simplifying multiple constitutes into only two hairpin reactants, and the high cell-delivering uniformity of the compact CCH system could eliminate the annoying crosstalk between the heterogeneous multiple-components.

As shown in **Figure S16A**, there are several possibilities for the three hairpins of the three-hairpin CHA-HCR system to enter cells, including that only one probe (**$mH_1$'** or **$mH_2$'** or **$mH_3$'**), two probes (**$mH_1$'** + **$mH_2$'** or **$mH_1$'** + **$mH_3$'** or **$mH_2$'** + **$mH_3$'**), and three probes (**$mH_1$'** + **$mH_2$'** + **$mH_3$'**) were transfected into cells simultaneously. The possibility of all probes entering cells is relatively low (about 1/7), leading to poor cell-delivering uniformity of the three-hairpin CHA-HCR system. However, there are three possibilities for the two hairpins of the CCH system entering cells, including that only one probe (**$mH_1$** or **$mH_2$**) and two probes (**$mH_1$** + **$mH_2$**) were transfected into cells simultaneously. The possibility of all probes entering cells is promoted to about 1/3 compared with the three-hairpin CHA-HCR system. A weak fluorescence of the three-hairpin CHA-HCR system was observed (**Figures S16B** and **S16C**), yet a significantly enhanced fluorescence of the CCH system was visualized (**Figures S16D** and **S16E**), indicating that high cell-delivering uniformity of the compact CCH system could assure more reliable site-specific signal response than three-hairpin CHA-HCR system.

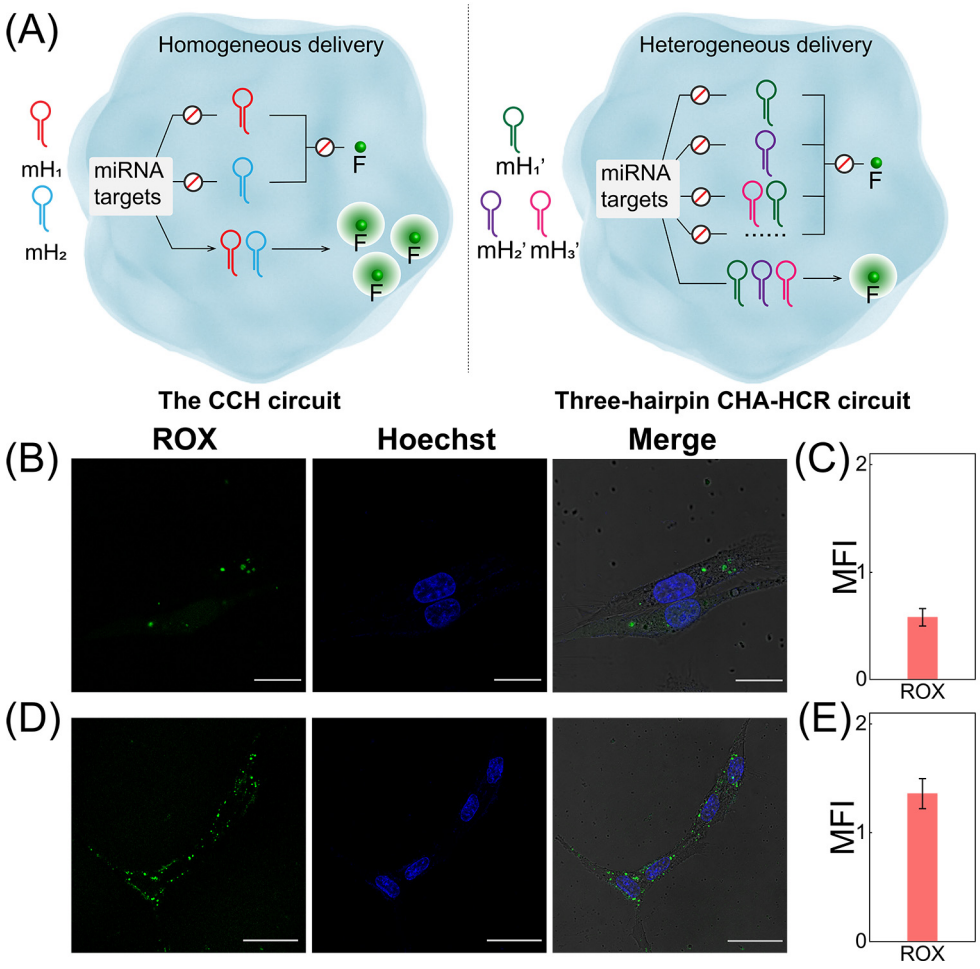


**Figure S16.** Imaging of the CCH system and three-hairpin CHA-HCR system. (A) The schematic illustration of probes delivery for the CCH system and three-hairpin CHA-HCR system. The possibility of all CCH probes entering cells is promoted to about 1/3 compared with the three-hairpin CHA-HCR system (about 1/7). (B) CLSM images of MDA-MB-231 cells treated with the three-hairpin CHA-HCR system. (C) The corresponding statistical histogram of MFI from **Figure S16B**. (D) CLSM images of MDA-MB-231 cells treated with the CCH system. (E) The corresponding statistical histogram of MFI from **Figure S16D**. Scale bar: 20 μm. Error bars represent one standard deviation for three independent experiments.

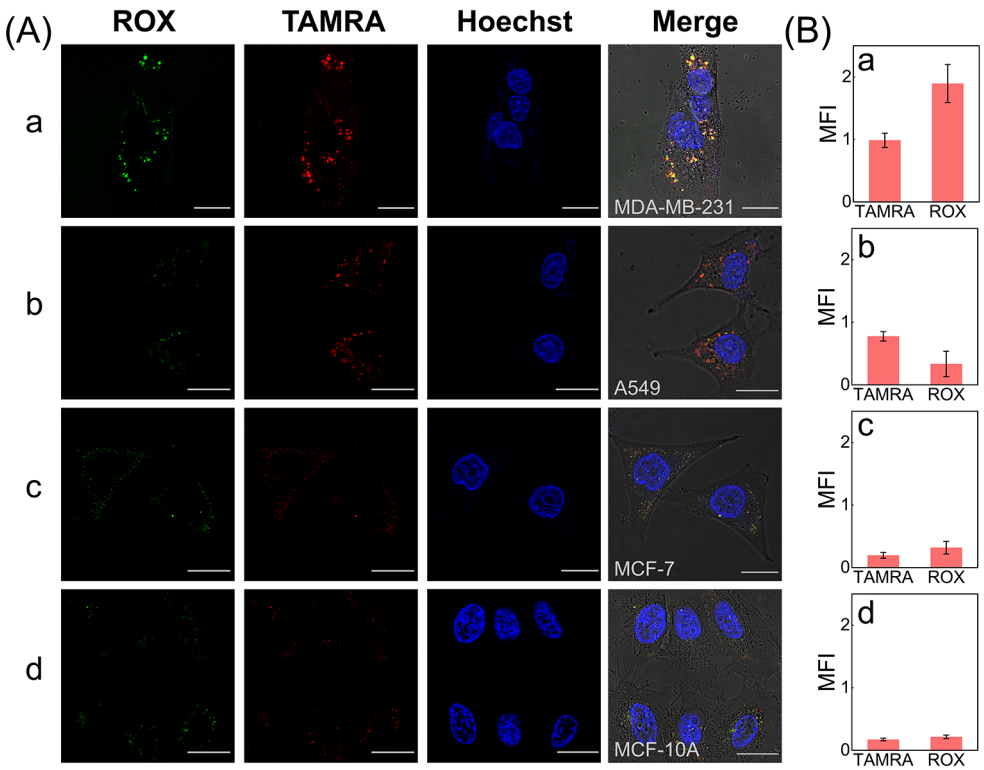


**Figure S17.** Imaging performance of the CCH circuit in different cells. (A) CLSM images of the CCH circuit treated in: (a) MDA-MB-231 cells, (b) A549 cells, (c) MCF-7 cells, and (d) MCF-10A cells. Scale bar: 20 μm. (B) The corresponding statistical histogram of MFI from **Figure S17A**. Error bars represent one standard deviation for three independent experiments.

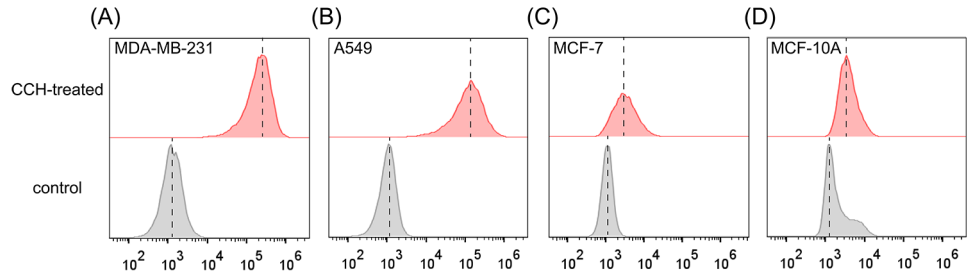


**Figure S18.** Flow cytometry analysis of TAMRA fluorescence in CCH-treated different cells (corresponding to **Figure 5C**). Flow cytometry analysis of the CCH circuit treated in: (A) MDA-MB-231 cells, (B) A549 cells, (C) MCF-7 cells, and (D) MCF-10A cells.

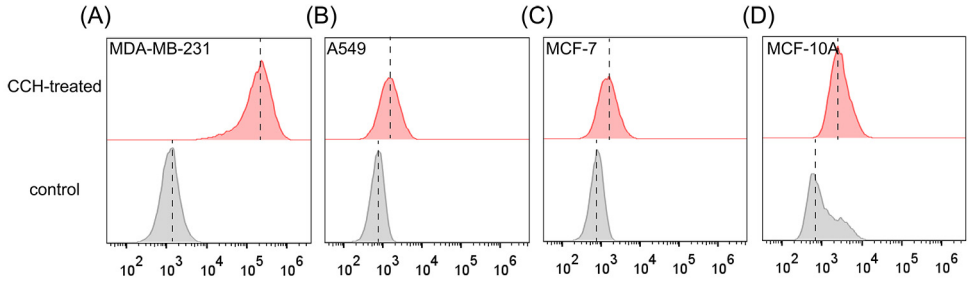


**Figure S19.** Flow cytometry analysis of ROX fluorescence in CCH-treated different cells (corresponding to **Figure 5E**). Flow cytometry analysis of the CCH circuit treated in: (A) MDA-MB-231 cells, (B) A549 cells, (C) MCF-7 cells, and (D) MCF-10A cells.

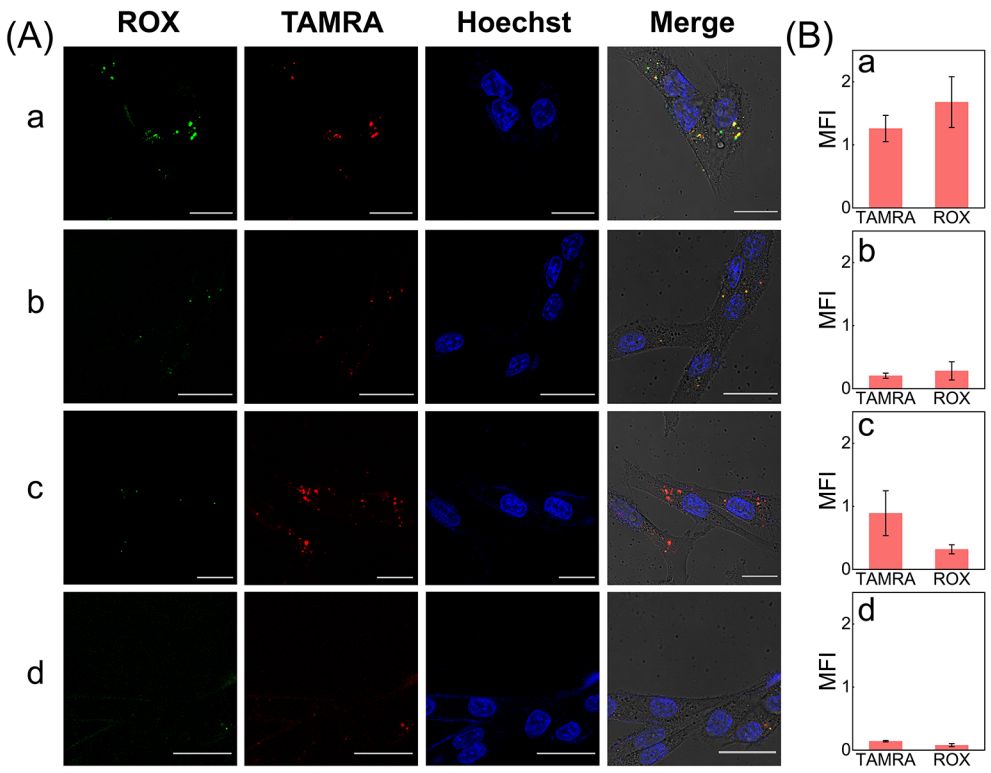


**Figure S20.** Imaging of MDA-MB-231 cells with different miRNAs expression profiles. (A) CLSM images of the compact CCH system in the MDA-MB-231 cells pre-treated with (a) no anti-miRNA, (b) anti-miR-155, (c) anti-miR-21, and (d) anti-miR-155 and anti-miR-21. (B) The corresponding statistical histogram of MFI from **Figure S20A**. Scale bar: 20 μm. Error bars represent one standard deviation for three independent experiments.